First-principles study of the orthorhombic mechanism for the $B3/B1$ high-pressure phase transition of ZnS

Michele Catti*
Dipartimento di Scienza dei Materiali, Università di Milano Bicocca, via Cozzi 53, 20125 Milano, Italy
(Received 29 November 2001; published 13 June 2002)

Ab initio periodic DFT-LCAO methods ($B3LYP$ and LDA functionals), at the all-electron level, were employed to study the atomic pathway of the zinc blende to rocksalt phase transition of ZnS. By the technique of constant pressure enthalpy minimization, the transformation mechanism based on a $Pmm2$ orthorhombic intermediate structure, recently proposed for SiC, was examined and compared to the traditional $R3m$ rhombohedral pathway. At the equilibrium pressure of 19 GPa, an activation enthalpy of 0.15 ($Pmm2$) against 0.50 ($R3m$) eV was obtained, confirming the orthorhombic mechanism to be definitely most favored also for a more ionic solid such as ZnS. The band gap is predicted to narrow progressively from zinc blende to rocksalt, with a parallel increase of the Zn to S charge transfer. Some structural and electronic features indicate a jumplike character of the transformation mechanism at about one third of the path.

DOI: 10.1103/PhysRevB.65.224115 PACS number(s): 61.50.Ah, 61.50.Ks, 62.50.+p, 64.70.Kb

I. INTRODUCTION

Molecular mechanisms of chemical reactions have been long investigated by quantum-mechanical calculations, so as to get insight into the microscopic aspects of chemical kinetics. On the other hand, only quite recently *ab initio* methods have begun to be applied to the study of atomic-scale transformation pathways in the solid state. Yet, predicting activation energies and other phenomelogical kinetic parameters on a first-principles basis is potentially very attractive for many crystal processes.

The simplest case is that of pressure-driven solid-solid phase transitions, which can be tackled by a straightforward static computational approach. The configurational space of intermediate metastable states is constrained by ideal lattice periodicity (defects are not taken into account), and within it least-enthalpy paths are searched for. A crucial role is played by symmetry lowering of the ''activated state,'' whose space group must be a subgroup of those of both end phases. Further, a few recent experimental techniques promise to be able to probe directly or undirectly the intermediate metastable states occurring in such transformations: compare the cases of x-ray diffraction peak profile analysis[1] and of time-resolved electronic spectroscopy coupled with shock wave techniques,[2,3] which were applied to study the CdSe and CdS wurtzite to rocksalt phase transitions, respectively.

The mechanisms of high-pressure phase transformations studied so far by ab initio methods concern the octahedral to cubic ($B1$ to $B2$)[4,5] and tetrahedral to octahedral ($B3$ or $B4$ to $B1$)[6–9] coordination changes in compounds with AB stoichiometry. In particular, with reference to the $B3/B1$ ($F43m$ zinc blende/ $Fm3m$ rocksalt) phase transition of SiC, we have been recently able to demonstrate that a pathway based on orthorhombic intermediate states is clearly favored, on energetic grounds, over the traditional rhombohedral mechanism.[9] This study is continued in the present work and extended to the same transformation for ZnS, where the chemical bonding is more ionic than in SiC, and thus the activated state in the kinetic process might show a different behavior.

Zinc sulfide is a wide-gap semiconductor of well known importance for applications in the fields of optical device technology: optical memories and visual displays are some of the devices based on this class of materials. Both ambient pressure polymorphs of ZnS (cubic zinc blende and hexagonal wurtzite) undergo a phase transition to the rocksalt structure at a comparatively low pressure, with respect to other AB semiconductors, in the range from 12 to 18 GPa according to different authors.[10–16] It seemed therefore interesting to check the results obtained previously for SiC, with a transition pressure approaching 100 GPa, on zinc sulfide. Further, the electronic and chemical bonding properties along the transformation pathway are investigated in the present case, as well as details of the structural changes of the intermediate states not taken into account in the SiC study. In particular, the higher ionicity of ZnS with respect to SiC suggests that charge transfer effects could play an important role in the transformation mechanism for the present compound.

Several previous first-principles investigations of ZnS are present in the literature, dealing mostly with the band structure simulation at ambient conditions;[17,18] predictions of the $B3/B1$ phase transition pressure are also reported in a recent study.[19] The theoretical method adopted in this paper is density-functional theory (DFT) coupled with use of an all-electron localized basis set of Gaussian-type atomic orbitals. This approach has proved successful for the *ab initio* modelling of a number of non-equilibrium Arrhenius-type crystal processes, including also ionic mobility in the solid state.[20]

II. COMPUTATIONAL METHOD

All quantum-mechanical calculations were carried out by the computer code CRYSTAL98,[21] implementing a periodic LCAO (linear combination of atomic orbitals) approach in which the self-consistent-field equations for one-electron eigenvalues and crystalline orbitals can be solved by use of a variety of Hamiltonians, which range from pure Hartree-Fock to pure DFT. Here the $B3LYP$ and LDA Hamiltonians are employed. The former is based on a ''hybrid'' combina-

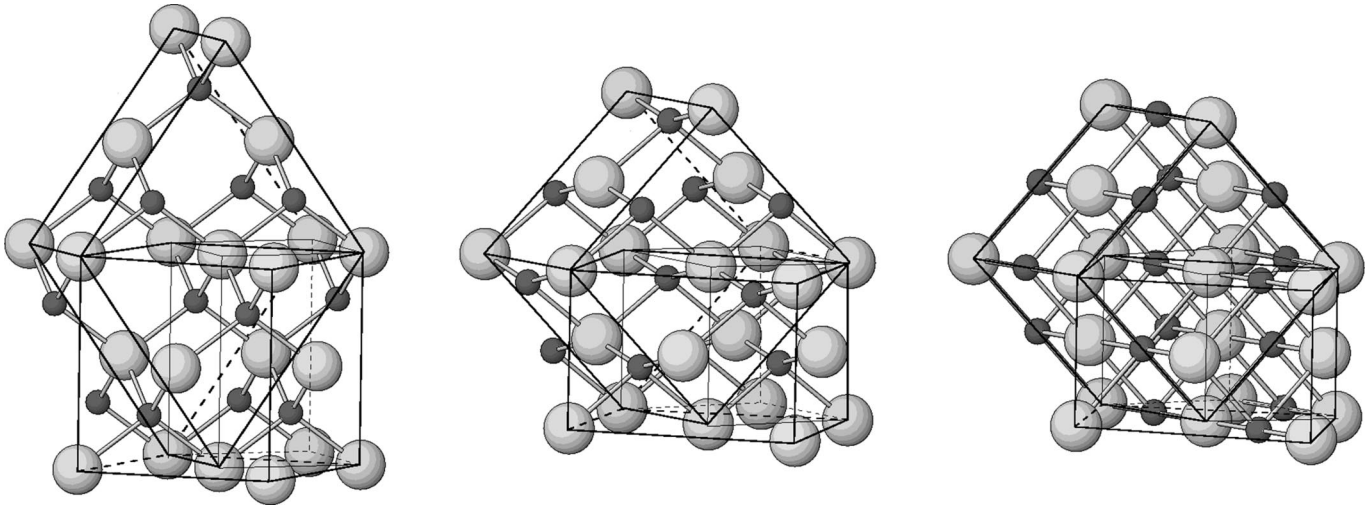

FIG. 1. Transformation path of the ZnS structure at $p=19$ GPa, from zinc blende (left) to $Pmm2$ intermediate state (middle) to rocksalt (right).

tion of 80% nonlocal Becke's[22] and 20% Hartree-Fock exchange potentials, and uses the gradient-corrected correlation functional of Lee-Yang-Parr,[23] according to the formula proposed by Becke.[24] The LDA (local-density-approximation) functional used is based on the Dirac-Slater[25] exchange and Perdew-Wang[26] correlation potentials.

An all-electron localized basis set, based on 31 (Zn) and 22 (S) atomic orbitals, was employed. The radial factors are expressed as linear combinations of Gaussian-type functions of the electron-nucleus distance, according to $8(s)64111(sp)41(d)$G and $8(s)6311(sp)1(d)$G contractions for zinc[27] and sulphur,[28] respectively. The exponents of the outer sp and d-type Gaussian functions were reoptimized by minimizing the total energy of the ZnS zinc blende crystal structure at the experimental configuration.

The level of numerical approximation in evaluating the Coulomb and exchange series appearing in the SCF equations for periodic systems is controlled by five tolerances.[21] These are related to estimates of overlap or penetration for integrals of Gaussian functions on different centres, which define cutoff limits for series summation. The values used in the present calculations are 10^{-6}, 10^{-6}, 10^{-6}, 10^{-6}, and 10^{-12}. The reciprocal space was sampled according to a regular sublattice defined by eight points in the Monkhorst grid (29 and 125 points in the irreducible Brillouin zones of the cubic and orthorhombic phases of ZnS, respectively). Convergence was checked with respect both to tolerances and to the number of Monkhorst points, and it was controlled by a threshold ($\Delta E=10^{-7}$ hartree per primitive unit cell) in the self-consistent-field cycles. In order to accelerate the SCF convergence, the technique of level shifter was often used: that enhances the energy difference between highest occupied and lowest empty states in the first cycles.

The structure optimizations were performed by the LoptCG routine written by C. Zicovich-Wilson, which is based on computation of numerical derivatives of the total energy with respect to structural variables, and subsequent processing by conjugate gradients. The routine was modified so as to minimize the enthalpy $H=E+pV$ at a given pressure, rather than the energy at zero pressure as in the ordinary case.

III. RESULTS AND DISCUSSION

A. Transition path and activation enthalpy

In a preliminary calculation, the total energies of the $B3$ and $B1$ phases of ZnS were computed by the $B3LYP$ method for a range of unit-cell volumes, and they were fitted to the Murnaghan equation of state obtaining $V_0=41.84$ (34.59) Å^3, $K_0=71.4$ (90.0) GPa, and $K'=4.0$ (3.9) for zinc blende (rocksalt). These results are in good agreement with experimental data:[16] $V_0=39.65$ (32.38) Å^3, $K_0=75.0$ (103.6) GPa, and K' fixed to 4 (4). Then, the phase transition pressure p_t was evaluated, by computing the enthalpy change $\Delta H_t=H$(rocksalt)-H(zinc blende) at different pressures and solving the $\Delta H_t(p)=0$ equation. The enthalpy of each phase was minimized against the cubic cell edge at every p value. By using the $B3LYP$ functional, calculations were carried out at $p=0$, 9.1, 18.3, 27.4, and 36.6 GPa. A parabolic fit yielded $\Delta H_t(p)=0.710-0.0410p+2.17\times10^{-4}p^2$, with p/GPa and H/eV, whence $p_t=19.3$ GPa. LDA results were obtained for $p=0$, 5.5, 11.0, 16.5, and 22.0 GPa, giving $\Delta H_t(p)=0.421-0.0396p+2.57\times10^{-4}p^2$, and $p_t=11.4$ GPa. The discrepancy between the $B3LYP$ and LDA predicted transition pressures is consistent with previous results of similar calculations,[9,29] and with the well known behavior of gradient-corrected (GGA, $B3LYP$) and LDA approximations in simulating the solid phase stabilities at variable pressure. Shortly, the LDA overestimate of binding energies is larger for denser phases, so that phase transition pressures are invariably predicted to be too low. On the other hand, gradient-corrected functionals usually overcorrect the LDA error, leading to the opposite effect of producing too high transition pressures. For the $B3/B1$ transition of ZnS, experimental results obtained by x-ray diffraction in static compression runs yield p_t values in a range from 12 to 18 GPa,[10–16] which is close to that between our LDA and $B3LYP$ data.

TABLE I. Unit-cell edges, volume and enthalpy (per formula unit) of the ZnS orthorhombic $Pmm2$ intermediate state between the $B3$ and $B1$ cubic end structures. Values computed by the DFT-$B3LYP$ functional vs the z fractional coordinate of Zn at $p=0$ (above, enthalpy zero $-59\,253.593$ eV) and at the equilibrium pressure of 19.3 GPa (below, enthalpy zero $-59\,249.041$ eV). The parameters of the I and II ($B3$- and $B1$-like) unit cells are also given.

z(Zn)	a (Å)	b (Å)	c (Å)	V (Å^3)	ΔH (eV)	a_{I} (Å)	γ_{I}(°)	a_{II} (Å)	γ_{II}(°)
0.250	3.897	3.897	5.511	41.8	0.000	5.511	90.0	6.750	70.5
0.275	3.993	3.835	5.497	42.1	0.040	5.536	87.7	6.703	69.8
0.300	4.110	3.794	5.391	42.0	0.152	5.593	85.4	6.592	70.3
0.325	4.238	3.779	5.230	41.9	0.319	5.678	83.4	6.452	71.7
0.350	4.480	3.862	4.616	39.9	0.483	5.915	81.5	6.019	79.8
0.375	4.690	3.881	4.193	38.2	0.597	6.088	79.2	5.713	85.6
0.400	4.888	3.810	3.918	36.5	0.665	6.197	75.9	5.465	88.4
0.425	5.000	3.780	3.800	35.9	0.702	6.268	74.2	5.360	89.7
0.450	5.110	3.710	3.711	35.2	0.709	6.315	72.0	5.247	90.0
0.475	5.165	3.659	3.668	34.7	0.710	6.330	70.6	5.181	89.9
0.500	5.172	3.657	3.657	34.6	0.713	6.334	70.5	5.172	90.0
0.250	3.669	3.669	5.189	34.9	0.000	5.189	90.0	6.355	70.5
0.275	3.810	3.577	5.104	34.8	0.031	5.226	86.4	6.233	70.0
0.300	3.996	3.551	4.834	34.3	0.108	5.346	83.3	5.998	72.6
0.325	4.313	3.703	4.125	32.9	0.152	5.685	81.3	5.543	83.8
0.350	4.492	3.732	3.820	32.0	0.151	5.840	79.4	5.340	88.7
0.375	4.618	3.688	3.677	31.3	0.132	5.910	77.2	5.208	90.2
0.400	4.728	3.625	3.581	30.7	0.105	5.958	75.0	5.096	90.7
0.425	4.832	3.554	3.526	30.3	0.074	5.998	72.7	5.006	90.5
0.450	4.882	3.510	3.500	30.0	0.031	6.013	71.4	4.957	90.2
0.475	4.897	3.490	3.486	29.8	0.004	6.013	71.0	4.933	90.1
0.500	4.918	3.478	3.478	29.7	0.000	6.024	70.5	4.918	90.0

The kinetic mechanism of phase transformation was examined, first of all, along the new orthorhombic $Pmm2$ pathway recently proposed for the same transition of SiC.[9] The unit cell of intermediate states contains two ZnS formula units, with fractional coordinates of the S atoms equal to 0,0,0 and $\frac{1}{2},\frac{1}{2},\frac{1}{2}$, and of Zn to $0,\frac{1}{2},z$ and $\frac{1}{2},0,z+\frac{1}{2}$. The z value, indicated hereafter as z(Zn), is assumed as order parameter or transition coordinate of the process. In the $Pmm2$ representation, the cubic $F\bar{4}3m$ zinc blende and $Fm\bar{3}m$ rocksalt end states are characterized by the constraints $a=b$, $c=\sqrt{2}a$, $z(\mathrm{Zn})=\frac{1}{4}$, and $b=c$, $a=\sqrt{2}b$, $z(\mathrm{Zn})=\frac{1}{2}$, respectively. Their unit cells are related to the $Pmm2$ one by the transformation matrices $[1-10|110|001]$ (zinc blende, cell I) and $[011|0-11|100]$ (rocksalt, cell II), whose rows represent the basis vector components of either I or II cell in terms of those of the orthorhombic unit cell. Of course, along the transformation path the I and II cells are distorted into a noncubic geometry with only two equal edges and two right angles, and their lattice constants are related to the orthorhombic ones according to $a_I=b_I=\sqrt{a^2+b^2}$, $c_I=c$, $\cos\gamma_I=[1-(b/a)^2]/[1+(b/a)^2]$, $a_{II}=b_{II}=\sqrt{b^2+c^2}$, $c_{II}=a$, $\cos\gamma_{II}=[1-(b/c)^2]/[1+(b/c)^2]$. In Fig. 1, the end structures and an intermediate state with $z(\mathrm{Zn})=0.375$ are shown, with all three kinds of unit cells outlined.

The total enthalpy of the $Pmm2$ structure of ZnS was minimized with respect to the unit-cell edges a, b, and c at values of the reaction coordinate z(Zn) ranging from 0.25 to 0.5 with steps of 0.025. The whole procedure was repeated at constant p values of 0, 9.1 and 19.3 (equilibrium pressure p_t) GPa, using the $B3LYP$ functional. Results for zero pressure and $p=p_t$ are reported in Table I, where the enthalpy changes with respect to the zinc blende end phase and the optimized lattice constants (also in the I and II reference frames) are given. The curves of ΔH vs z(Zn) are shown in Fig. 2 for all three pressure values considered. Activation enthalpies of the phase transition in the forward ($B3$ to $B1$, $\Delta H_a^{\rightarrow}$) and backward ($B1$ to $B3$, $\Delta H_a^{\leftarrow}$) directions are given, for every pressure, by the enthalpy differences between the maximum and the $z=0.25$ or $z=0.5$ end point, respectively. The constraint $\Delta H_a^{\rightarrow}-\Delta H_a^{\leftarrow}=\Delta H_t$ must hold, so that at the equilibrium pressure p_t we have that $\Delta H_a^{\rightarrow}=\Delta H_a^{\leftarrow}=\Delta H_{a,t}$. By inspection of Fig. 2, a behavior similar to that shown by silicon carbide[9] appears: $\Delta H_a^{\leftarrow}$ is vanishing at zero pressure, but increases with p till it equals $\Delta H_a^{\rightarrow}$ at p_t; $\Delta H_a^{\rightarrow}$ decreases from ΔH_t to $\Delta H_{a,t}$ as p rises from zero to the equilibrium value p_t. The parabola passing through the three p points considered is $\Delta H_a^{\rightarrow}=0.713-0.04215p+6.83\times10^{-4}p^2$, with eV and GPa as units. From this expression, the forward activation volume (i.e., the volume dif-

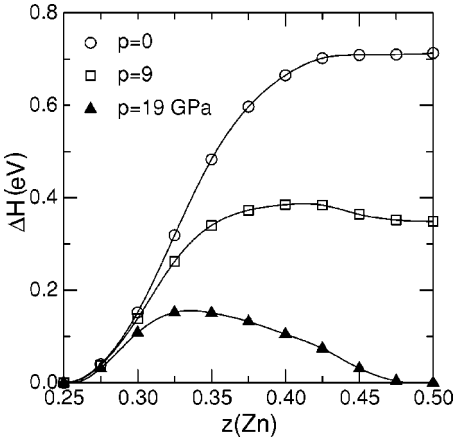

FIG. 2. Enthalpy change (one ZnS formula unit) with respect to the zinc blende phase along the $Pmm2$ transformation pathway to rocksalt, plotted versus the zinc z fractional coordinate at different pressures. Results obtained by the $B3LYP$ functional.

ference between the bottleneck state along the reaction pathway and the end state stable at low pressure) can be obtained as $\Delta V_a^{\rightarrow} = d\Delta H_a^{\rightarrow}/dp = -6.75 + 0.219p$, with units of GPa and Å^3. Forward and backward values are related according to $\Delta V_a^{\rightarrow} - \Delta V_a^{\leftarrow} = \Delta V_t$, where ΔV_t is the volume difference between the two end states. In Fig. 2 it appears that, on raising pressure, the z(Zn) abscissa of the enthalpy maximum (bottleneck state) decreases, so that $|\Delta V_a^{\rightarrow}|$ must decrease as well, consistently with the behavior of $\Delta V_a^{\rightarrow}(p)$ obtained above. Further, the $\Delta H(z)$ curve at $p_t = 19$ GPa has a quite asymmetrical shape, with the maximum at $z(\mathrm{Zn}) = 0.337$; this indicates that deforming the zinc blende structure along the reaction pathway is enthalpically more expensive than the opposite way starting from the rocksalt end phase.

The $B3/B1$ transformation of ZnS was also explored according to the $R3m$ mechanism, by minimizing the enthalpy with respect to the a and c edges of the hexagonal unit cell related to the I cell by the matrix $[-\frac{1}{2}\frac{1}{2}0|0-\frac{1}{2}\frac{1}{2}|111]$. The asymmetric unit contains S at 0,0,0 and Zn at 0,0,z, with the reaction coordinate z(Zn) moving from 0.25 to 0.5 also in this case. With respect to cell I, the mechanism corresponds to a shift of Zn along the cube diagonal from $\frac{1}{4},\frac{1}{4},\frac{1}{4}$ to $\frac{1}{2},\frac{1}{2},\frac{1}{2}$, with an intermediate rhombohedral deformation of the cubic cell. Calculations were performed at the equilibrium pressure of 19.3 GPa; the $\Delta H(z)$ curve obtained is shown in Fig. 3 and therein compared to the corresponding one for the $Pmm2$ pathway. It is clear that the $R3m$ mechanism, with an activation enthalpy of 0.50 eV, should be discarded in favor of the $Pmm2$ path showing a value of only 0.15 eV. This confirms what found previously for the corresponding transformation of SiC, where, however, the activation enthalpies were much larger (0.75 and 2.10 eV for the $Pmm2$ and $R3m$ mechanisms, respectively), as a consequence of the higher transition pressure of 92 GPa. Further, the $R3m$ curve is symmetrical, indicating a bottleneck state exactly half way between the end phases at variance with the features of the $Pmm2$ pathway. Both curves were also recomputed using the LDA instead of $B3LYP$ functional, at the corresponding

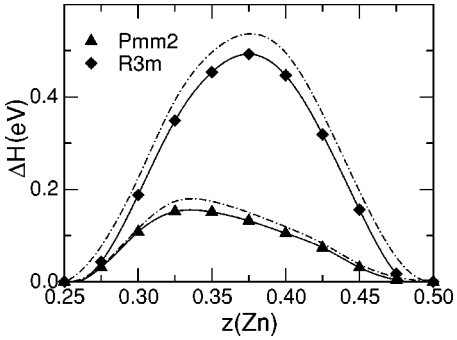

FIG. 3. Enthalpy changes along the $Pmm2$ and $R3m$ transition paths, predicted by the $B3LYP$ (full lines) and LDA (dashed-dotted lines) functionals at the equilibrium pressure p_t (19 and 11 GPa for the $B3LYP$ and LDA cases, respectively).

transition pressure of 11.4 GPa. The results, shown as dashed-dotted lines in Fig. 3, are fully consistent with those previously discussed; a slight increase of the activation enthalpy is observed ($Pmm2$ 0.17 and $R3m$ 0.54 eV), which is however quite minor if compared to the large difference between the $B3LYP$ (19 GPa) and LDA (11 GPa) equilibrium pressures. Thermodynamics seems to be affected to a much larger extent than kinetics by neglect or inclusion of nonlocal corrections to the electron density functional.

An explanation of the lower energetic cost of the $Pmm2$ over the $R3m$ mechanism for the zinc blende to rocksalt transformation can be obtained by considering the changes of chemical bonding undergone by the Zn atom along the two pathways (Fig. 4). In the rhombohedral mechanism, zinc moves along the line connecting the centers of a sulphur tetrahedron and of an adjacent octahedron sharing a triangular face. The bottleneck state is achieved exactly at midway, in the face center, where Zn attains a triangular coordination by breaking one of the four Zn-S bond. This is consistent with the symmetrical shape of the $\Delta H(z)$ curve in Fig. 3. On the other hand, the orthorhombic pathway is based on the progressive deformation of a pair of S tetrahedra sharing an edge into an octahedron, with the Zn atom moving from a tetrahedron center to the middle point of that edge, becoming the octahedron center. By that way, none of the four Zn-S bonds are broken, but two extra ones are added progressively.

At a given pressure, the structural evolution of the $Pmm2$ intermediate states along the transformation pathway could be defined by the dependence of the unit-cell edges a, b, and c on the reaction coordinate z(Zn), obtained by enthalpy

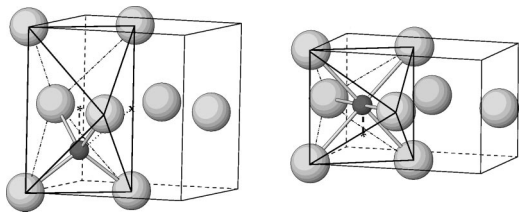

FIG. 4. Coordination change of Zn (small sphere) from tetrahedral to octahedral along the $Pmm2$ pathway (thick dashed line). The $R3m$ path is denoted by a dotted line in the left-hand picture.

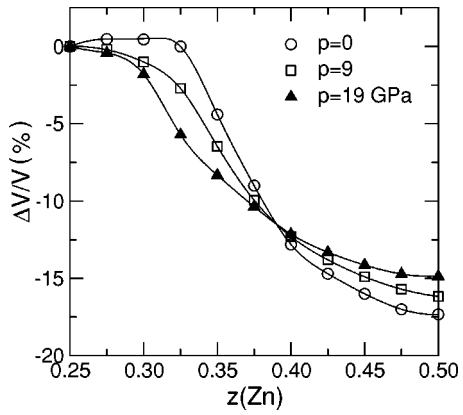

FIG. 5. Percent volume change (with respect to the zinc blende phase) along the $Pmm2$ transformation pathway, plotted versus the zinc z fractional coordinate at different pressures. Results obtained by the $B3LYP$ functional.

minimization. However, it is more convenient to separate extensive from intensive configurational variables, by choosing the unit-cell volume in the first class and two cell edge ratios in the second one. We therefore adopt a representation based on the volume change (per ZnS formula unit) ΔV with respect to the zinc blende-type end phase, and on the b/a and b/c ratios, which are plotted as functions of $z(\mathrm{Zn})$ in Figs. 5 and 6, respectively, for the three pressure values considered in the calculations. In Fig. 5, for each curve the difference between the end values at $z=0.5$ and 0.25 gives $\Delta V_t/V$, and the value corresponding to the abscissa $z(\mathrm{Zn})$ of the enthalpy maximum in the corresponding curve of Fig. 2 yields the relative activation volume $\Delta V_a^{\rightarrow}/V$. All curves present inflection points the closer to the starting ($B3$) configuration the higher the pressure, with a slope decreasing with increasing p, so that at $p=p_t$ the volume change along the transformation path is smoother. The behavior of the cell edge ratios (Fig. 6) is peculiar, because b/a varies very smoothly with the reaction coordinate, whereas b/c has a pronounced jumplike character independently of pressure. This can be interpreted by remembering that b/a and b/c are related to the

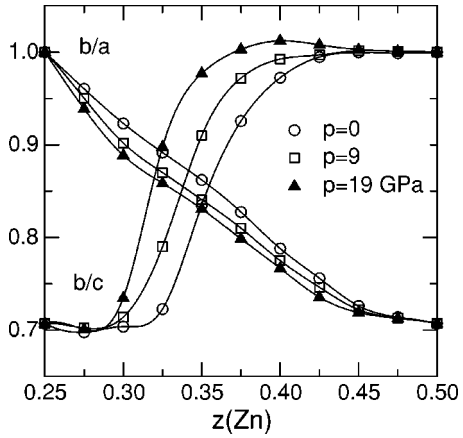

FIG. 6. Unit-cell ratios b/a and b/c of the orthorhombic $Pmm2$ intermediate state, plotted versus the zinc z fractional coordinate at different pressures.

angles γ_{I} and γ_{II} of the deformed cubic cells of the zinc blende (I) and rocksalt (II) structures, respectively. Therefore, the angular deformation of the $B3$ cell is approximately continuous, but that of the $B1$ one occurs nearly abruptly in the first stage of the transformation path (see also Table I). A remarkable feature is that the inflection points of the b/c and ΔV curves occur at approximately the same $z(\mathrm{Zn})$ values, for corresponding pressures, and such ''critical'' values of the reaction coordinate (0.35, 0.34, and 0.32 for $p=0$, 9 and 19 GPa, respectively) decrease as p rises.

The question can be raised whether the $Pmm2$ nonequilibrium state of ZnS, characterized here on theoretical grounds, may be related structurally to any known stable phase of other binary compounds. By inspection of the high-pressure polymorphs of III-V semiconductors, attractive candidates appear to be the orthorhombic phases InSb(IV) (or P4) (Refs. 30 and 31) and GaAs(II),[32] which are stable in the pressure ranges 2 to 6 and 17 to 24 GPa, respectively. On the basis of x-ray diffraction results, the same $Pmm2$ structure was proposed in both cases, with two atoms per unit cell at 0,0,0 and at $0,\frac{1}{2},z$; the z coordinate was refined to 0.387 (InSb) and to 0.35 (GaAs). However, this structure differs from $Pmm2$-ZnS and $Pmm2$-SiC because the two atoms at $\frac{1}{2},\frac{1}{2},\frac{1}{2}$ and at $\frac{1}{2},0,z+\frac{1}{2}$ are missing, so that only half of the unit cell content is present, with respect to our nonequilibrium state. With reference to Fig. 1 (middle), this corresponds to removing every second (001) layer of S and Zn atoms. It should be added that the structural model of InSb(IV) and GaAs(II) is not able to distinguish the chemical nature of the two atoms in the unit cell, because of their similar x-ray scattering factors, and that a superstructure variant is probable at least for InSb/IV).[31] We thus conclude that, in spite of apparent similarities, the two structures are different.

B. Density of states and charge transfer

The density of one-electron energy states (DOS) has been computed for the zinc blende and rocksalt end phases and for the intermediate $Pmm2$ state with $z(\mathrm{Zn})=0.35$, both at $p=0$ and at the equilibrium pressure $p=p_t$. Results of the $B3LYP$ calculation at $p_t=19.3$ GPa are shown in Fig. 7. In all three phases, the valence band is built up mainly by sulphur sp states, with a minor presence of zinc d levels; a very high and sharp band with opposite composition (mostly Zn d with some S sp states) is located slightly below. The conduction band has a prevalent Zn-d character. The most striking feature is that, at constant pressure, the band gap E_g shrinks steadily along the $B3$-$B1$ transformation path, with a sharp fall in the first part of the process, but without closing completely at the rocksalt end. While the valence band is little affected, the conduction band changes substantially along the pathway, becoming much flatter in the proximity of the gap. Further, the intermediate $Pmm2$ state at $z=0.35$ shows an electronic structure much more similar to that of the rocksalt than of the zinc blende phase, consistently with the behavior of the lattice deformation (see the b/c curve at 19 GPa in Fig. 6). The band gap narrowing observed along the $B3$-$B1$ pathway is clearly related to the volume decrease

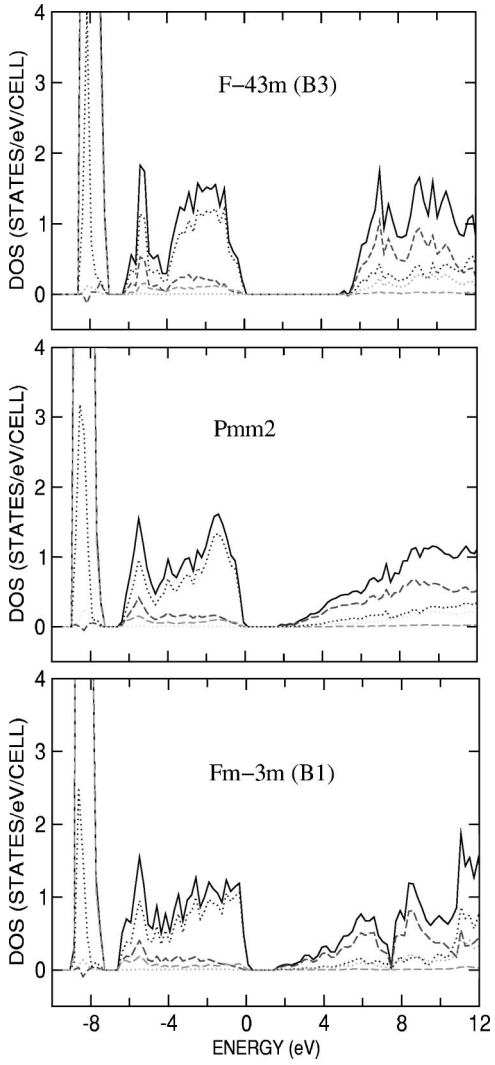

FIG. 7. Density of states of ZnS computed ($B3LYP$ functional) at 19 GPa for the zinc blende (above), intermediate orthorhombic [$z(\mathrm{Zn})=0.35$, middle] and rocksalt (below) structures along the transformation pathway. Total DOS (full lines), and projections onto the S sp states (dotted lines) and Zn d states (dashed lines) are shown.

occurring parallely (Fig. 5), which engenders an overall bond length contraction and increases the coordination number from 4 to 6.

Values of the band gap, computed by both the $B3LYP$ and LDA functionals at $p=p_t$ and at $p=0$, are reported in Table II. Pressure appears to act upon E_g differently, according to the degree of advancement of the transformation: the gap decreases with increasing p in the final ($B1$) and intermediate stages of the phase transition, but it increases in the starting structural configuration ($B3$). The behavior of the ZnS zinc blende phase, whose band gap is predicted to widen under pressure, is at variance with the E_g lowering of many materials upon volume contraction, but is fully confirmed by optical measurements at high pressure.[16] In particular, theoretical $B3LYP$ results for zinc blende ZnS yield a coefficient of band gap increase on compression $D=\Delta E_g/(\Delta V/V)$ equal to -6.0 eV, which compares very favorably with the

TABLE II. Band energy gaps (eV) of the cubic end and orthorhombic intermediate structures of ZnS, computed at $p=p_t$ and at room pressure, and compared to other theoretical and experimental values from the literature.

		$F\bar{4}3m$ $z(\mathrm{Zn})=0.25$	$Pmm2$ 0.35	$Fm\bar{3}m$ 0.50
$B3LYP$	$p_t=19$ GPa	4.8	1.6	1.1
LDA	$p_t=11$ GPa	3.0	0	0
exp. [a]	$p_t=15$ GPa	4.3		~ 2
$B3LYP$	$p=0$	3.9	2.0	1.3
LDA	$p=0$	2.5	0	0
LDA-PP [b]	$p=0$	2.0		0
SIC-PP [c]	$p=0$	3.7		0.2
GWA [d]	$p=0$	4.0		
exp. [e]	$p=0$	3.7-3.8		

[a]Reference 16.
[b]Reference 18.
[c]Reference 18,19.
[d]Reference 17.
[e]Reference 16,36.

experimental value of -5.0 eV,[16] taking also into account that, because of experimental problems, ''the gap energies at higher pressures are considered to give the lower limit for the true value of the gap.''[16] A satisfactory agreement is observed, correspondingly, also between the theoretical $B3LYP$ and experimental absolute E_g value of the $B3$ and $B1$ phases of ZnS at the transition pressure (Table II), with consideration of the p_t difference between theory and experiment. As for the $B1$ phase, the measured band gap[16] was reported with a large uncertainty, and in previous work such phase had even believed to be conducting, so that our predicted value has a particular relevance.

Questions may be raised about the theoretical reliability of band gaps computed within the DFT approach, as it is well known that one-particle eigenvalues in DFT calculations do not formally correspond to excitation energies. Further, LDA results usually give too small gaps, and inclusion of gradient corrections (GGA) is not able to cure this drawback satisfactorily. Better approximations to the band gaps can be obtained by methods more expensive computationally, such as GW perturbation theory[33] and quantum Monte Carlo (QMC).[34] Also inclusion of the self-interaction correction (SIC) in LDA calculations with pseudopotential (PP) plane wave basis set has given encouraging results.[18,19] However, it has been shown recently that use of standard DFT with hybrid functionals such as $B3LYP$, where the exchange potential is an empirically-weighted mixture of GGA and Hartree-Fock contributions, can produce band gaps of the same quality of those given by the more sophisticated methods mentioned above.[35] This is illustrated just by the case of room pressure E_g values of zinc blende ZnS (Table II). The experimental results therein reported come from optical absorption measurements performed at room temperature (3.67 eV) (Ref. 16) and at 14 K (3.78 eV);[36] theoretical results from a variety of computational techniques are also included for comparison with our own data. It is clear that the $B3LYP$

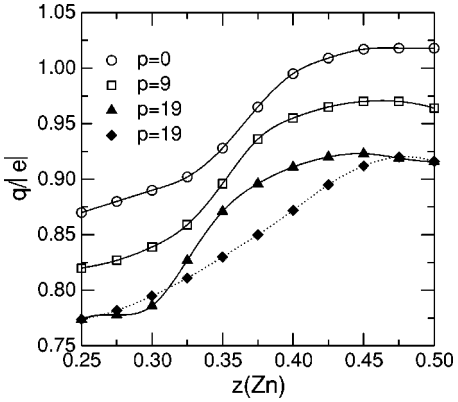

FIG. 8. Zinc Mulliken charge plotted versus the z fractional coordinate along the $Pmm2$ (full lines) and $R3m$ (dotted line) transition paths, at different pressures.

band gap agrees very well with experiment, and is close to values obtained by the best theoretical techniques. Further, concerning the rocksalt phase, the $B3LYP$ result compares much better with experiment than the value computed by the SIC-PP method.[19] As observed previously,[35] this good performance of the hybrid functional is probably fortuitous as due to some cancelling of opposite errors, but is anyway systematic for a large class of compounds, so as to attain an outstanding practical importance.

A different point of view on the change of electronic structure of ZnS along the phase transition path can be obtained by considering the Mulliken atomic charge $q(\mathrm{Zn})$ or $q(\mathrm{S})=-q(\mathrm{Zn})$. At zero pressure, the $B1$ and $B3$ phases give $q(\mathrm{Zn})=0.87$ and $1.02|e|$, respectively, to be compared with $q(\mathrm{Si})=0.34$ and $0.52|e|$ in the corresponding phases of SiC. Such values prove clearly ZnS to be much more ionic than silicon carbide. In Fig. 8, $q(\mathrm{Zn})$ is plotted against the reaction coordinate at different pressures, showing a steadily increasing behavior. This indicates a growing charge transfer within the Zn-S chemical bonding, related to the progressive increase of coordination number from 4 to 6. Further, each of the three $Pmm2$ curves has an ''s-like'' shape similar to that observed for the structural parameters b/c (Fig. 6) and $\Delta V/V$ (Fig. 5). Also the abscissae of the inflection points are close to those of the corresponding b/c and $\Delta V/V$ curves. Therefore, the $Pmm2$ transformation mechanism is confirmed to have a partially discontinous nature, not only with its structural but also with its electronic features (see also the band gap behavior discussed above). Interestingly, things are quite different for the $R3m$ mechanism, where Mulliken charges increase continuously along the pathway. Applied pressure has the effect of decreasing the charge transfer throughout the transformation, and of shifting the inflection point towards the zinc blende end, just as observed for the b/c and $\Delta V/V$ curves.

IV. CONCLUSIONS

The high-pressure transformation of ZnS from zinc blende to rocksalt structure has been shown to follow a $Pmm2$ orthorhombic pathway similar to that recently demonstrated for silicon carbide, although their transition pressures are very different and the first compound is much more ionic than the second one. First-principles calculations based on density-functional theory, and employing all-electron basis sets and a hybrid exchange-correlation potential ($B3LYP$), are confirmed to be a powerful and reliable tool for studying the kinetic mechanisms of solid-solid phase transitions at high pressure. In particular, activation enthalpies and activation volumes can be predicted straightforwardly, opening the way to a systematic determination of the least-enthalpy atomic pathways in such transformations. This may be a source of suggestions for new experiments and measurement techniques in the field of solid state kinetics. Another important result obtained is the prediction of band gap narrowing of ZnS along the transformation path, and of the different effect of pressure on the band gaps of the two end phases. This point will be investigated further in future work, also in connection with the zinc-sulphur charge transfer indicated by the dependence of Mulliken charges on the reaction coordinate and on pressure. Eventually, both the electronic (band gap and charge transfer) and structural (b/c ratio and volume change) predicted evolutions point out that the transformation rate is maximum at about one third of the pathway from zinc blende to rocksalt, with inflection points of all such quantities at a critical value of the reaction coordinate in the range 0.32–0.33 (at the equilibrium pressure). The role of charge transfer along the transition path is more important in ZnS than in SiC, consistent with the less covalent character of chemical bonding.

ACKNOWLEDGMENTS

This research was supported by a MURST-COFIN (Roma) grant, and by computing facilities from CINECA (Bologna).

*Electronic address: catti@mater.unimib.it

[1] J. N. Wickham, A. B. Herhold, and A. P. Alivisatos, Phys. Rev. Lett. **84**, 923 (2000).

[2] M. D. Knudson and Y. M. Gupta, Phys. Rev. Lett. **81**, 2938 (1998).

[3] M. D. Knudson, Y. M. Gupta, and A. B. Kunz, Phys. Rev. B **59**, 11 704 (1999).

[4] A. Martín-Pendás, V. Luaña, J. M. Recio, M. Florez, E. Francisco, M. A. Blanco, and L. N. Kantorovich, Phys. Rev. B **49**, 3066 (1994).

[5] C. E. Sims, G. D. Barrera, N. L. Allan, and W. C. Mackrodt, Phys. Rev. B **57**, 11 164 (1998).

[6] K. Karch, F. Bechstedt, P. Pavone, and D. Strauch, Phys. Rev. B **53**, 13 400 (1996).

[7] M. A. Blanco, J. M. Recio, A. Costales, and R. Pandey, Phys. Rev. B **62**, 105599(R) (2000).

[8] S. Limpijumnong and W. R. L. Lambrecht, Phys. Rev. Lett. **86**, 91 (2001).

[9] M. Catti, Phys. Rev. Lett. **87**, 035504 (2001).

[10] G. A. Samara and H. G. Drickamer, J. Phys. Chem. Solids **23**, 457

(1962).
[11] G. J. Piermarini and S. Block, Rev. Sci. Instrum. **46**, 973 (1975).
[12] T. Yagi and S. Akimoto, J. Appl. Phys. **47**, 3350 (1976).
[13] S. C. Yu, I. L. Spain, and E. F. Skelton, Solid State Commun. **25**, 49 (1978).
[14] A. Onodera and A. Ohtani, J. Appl. Phys. **51**, 2581 (1980).
[15] S. Desgrenier, L. Beaulieu, and I. Lepage, Phys. Rev. B **61**, 8726 (2000).
[16] S. Ves, U. Schwarz, N. E. Christensen, K. Syassen, and M. Cardona, Phys. Rev. B **42**, 9113 (1990).
[17] M. Oshikiri and F. Aryasetiawan, Phys. Rev. B **60**, 10 754 (1999).
[18] D. Vogel, P. Kruger, and J. Pollmann, Phys. Rev. B **54**, 5495 (1996).
[19] A. Qteish, J. Phys.: Condens. Matter **12**, 5639 (2000).
[20] M. Catti, Phys. Rev. B **61**, 1795 (2000).
[21] V. R. Saunders, R. Dovesi, C. Roetti, M. Causà, N. M. Harrison, R. Orlando, and C. M. Zicovich Wilson, *CRYSTAL98: User's manual* (University of Torino, Italy, and CLRC Daresbury Laboratory, UK, 1999).
[22] A. D. Becke, Phys. Rev. A **38**, 3098 (1988).
[23] C. Lee, W. Young, and R. G. Parr, Phys. Rev. B **37**, 785 (1988).
[24] A. D. Becke, J. Chem. Phys. **98**, 5648 (1993).
[25] P. A. M. Dirac, Proc. Cambridge Philos. Soc. **26**, 376 (1930).
[26] J. Perdew and Y. Wang, Phys. Rev. B **45**, 13 244 (1992).
[27] E. Jaffe and A. C. Hess, Phys. Rev. B **48**, 7903 (1993).
[28] A. Re, Basis sets compilation, CRYSTAL98, 1999.
[29] M. Catti, Phys. Chem. Miner. **28**, 729 (2001).
[30] C. A. Vanderborgh, Y. K. Vohra, and A. L. Ruoff, Phys. Rev. B **40**, 12 450 (1989).
[31] R. J. Nelmes, M. I. McMahon, P. D. Hatton, J. Crain and R. O. Piltz, Phys. Rev. B **47**, 35 (1993).
[32] S. T. Weir, Y. K. Vohra, C. A. Vanderborgh, and A. L. Ruoff, Phys. Rev. B **39**, 1280 (1989).
[33] L. Hedin, Phys. Rev. **139**, A796 (1965).
[34] D. Ceperley, G. Chester, and M. Kalos, Phys. Rev. B **16**, 3081 (1971).
[35] J. Muscat, A. Wander, and N. M. Harrison, Chem. Phys. Lett. **342**, 397 (2001).
[36] *Data in Science and Technology: Semiconductors Other than Group IV Elements and III-V Compounds* (Springer Verlag, Berlin, 1992).